Propagation of intense and short circularly polarized pulses in a molecular gas: From multiphoton ionization to nonlinear macroscopic effects

M. Lytova* and E. Lorin†
School of Mathematics and Statistics, Carleton University, Ottawa, Canada K1S 5B6

A. D. Bandrauk‡
Laboratoire de chimie théorique, Faculté des Sciences, Université de Sherbrooke, Sherbrooke, Canada J1K 2R1
(Received 24 March 2016; published 25 July 2016)

We present a detailed analysis of the propagation dynamics of short and intense circularly polarized pulses in an aligned diatomic gas. Compared to linearly polarized intense pulses, high harmonic generation (HHG) and the coherent generation of attosecond pulses in the intense-circular-polarization case are a new research area. More specifically, we numerically study the propagation of intense and short circularly polarized pulses in the one-electron H_2^+ molecular gas, using a micro-macro Maxwell–Schrödinger model. In this model, the macroscopic polarization is computed from the solution of a large number of time-dependent Schrödinger equations, the source of dipole moments, and using a trace operator. We focus on the intensity and the phase of harmonics generated in the H_2^+ gas as a function of the pulse-propagation distance. We show that short coherent circularly polarized pulses of same helicity can be generated in the molecular gas as a result of cooperative phase-matching effects.

DOI: 10.1103/PhysRevA.94.013421

I. INTRODUCTION

We study in this paper the highly nonlinear effects of propagation of intense and short circularly polarized (CP) pulses in a one-electron H_2^+ molecular gas. This work is in particular motivated by interest in circular filamentation [1], and more generally by the generated effects, at the macroscopic level, of molecules subject to intense and short few-cycle CP light. We simulate the evolution of the intensity and the phase of the generated odd time harmonics during the laser-molecule interaction as a function of the propagation length of the pulse in the gas. This is possible by using the Maxwell–Schrödinger-plasma (MASP) propagation model and code which was presented in several papers [2–5]. The MASP equations consist of the coupling of (i) macroscopic Maxwell equations modeling laser-pulses interacting with (ii) many laser-molecule time-dependent Schrödinger equations (TDSEs) from which are deduced by using a trace operator, the macroscopic polarization from the total-laser-induced molecular dipole moments.

High harmonic generation (HHG) in atomic or molecular gases by high-intensity ultrashort linearly polarized (LP) laser pulses is currently the main method for producing coherent extreme ultraviolet and attosecond (as) pulses [6]. This is based on a universal model of electron-recollision with a maximum harmonic energy,

$$N\hbar\omega_0 = I_p + 3.17U_p, \tag{1}$$

where I_p is the ionization potential of the atom or molecule, $U_p = e^2E^2/(4m\omega_0^2)$ is the ponderomotive energy of the electron in an oscillatory field $E(t)$ of maximum intensity $I = eE^2/8\pi$ and frequency ω_0 [7–13]. Molecules offer an interesting medium because both ionization and recombination steps are dependent on the particular symmetry of the highest occupied molecular orbital (HOMO) and orientation [10–12,14]. Furthermore, at large distances, stretched or dissociated molecules offer the possibility of obtaining harmonics well beyond the $3.17U_p$ cutoff law (1) [10,15,16]. The recombination LP model allows us to perform a full tomographic reconstruction of the HOMO at a high degree of spatial alignment of the molecules [17–19]. For LP pulses the mathematical steps in structural retrieval from HHG are based upon the strong-field approximation (SFA), a single active electron (SAE) model, and a three-step process [7,8]: (i) tunneling ionization with zero initial electron velocity; (ii) acceleration in the laser field $E(t)$; (iii) recombination back into the bound electronic state. This simple three-step model can be shown to always produce a maximum return energy predicted by Eq. (1), even with nonzero initial velocity upon ionization [9]. Several important questions still remain open, such as the influence of the intense laser field upon the bound electronic states upon recombination [20], depletion of the initial ground state [21], the influence of the Coulomb potential on the continuum electron states [22]; all effects neglected in SFA. Finally, it is important to consider macroscopic propagation effects because these lead to interesting phenomena such as filamentation [23,24] with the conclusion that ionization dynamics can strongly influence the synthesis of isolated attosecond pulses [25]. We focus in this paper on the single-electron H_2^+ system, which nevertheless involves coupled electron-nuclear motion beyond the Born–Oppenheimer approximation [26]. For this H_2^+ system, a previous TDSE simulation with exact non-Born–Oppenheimer solutions lead to enhanced ionization and HHG in the presence of an attosecond extreme ultraviolet (XUV) and infrared (IR) fs pulse with the resulting efficient generation of attosecond pulses [27]. A first Maxwell-TDSE

*mariannalytova@cmail.carleton.ca
†elorin@math.carleton.ca
‡Centre de Recherches Mathématiques, Université de Montréal, Montréal, Canada H3T 1J4; andre.bandrauk@usherbrooke.ca

equation for this system was then developed, based on a slowly varying envelop approximation (SVEA), leading to a first-order partial differential equation [28]. Such an approach neglects ground-state depletion due to ionization, neglects backward propagation, and is therefore appropriate only for low field strengths. It was nevertheless found that initial attosecond pulses could be shortened further in time through the resultant HHG attosecond pulses produced nonlinearly in the presence of an intense IR fs pulse [29]. Later, a Maxwell-TDSE model was developed in Ref. [30], where aligned one-dimensional (1-d) $H_2{}^+$ molecules were subject to intense short LP fields. The present work is an extension of Ref. [30] in the case of CP pulses.

For circularly polarized fields interacting with atoms, recollision is predicted from classical models to be absent and requires pairs of co- or counter-rotating circular pulses [31–33]. We show that including propagation effects can produce HHG with single CP intense pulses in molecular systems. In this paper we address the problem of attosecond-pulse generation and propagation by HHG in an aligned molecular medium subject to CP pulses [34–36]. The molecules are assumed to be aligned, and with all the same orientation, thanks to a first low-intensity pulse. We emphasize that this is a not a constraint of the model and random orientation of the molecules could also be considered. The propagation effects on the generated harmonic intensities were specifically analyzed, such as the coherent generation of high-energy photons as a function of the pulse propagation length.

We conclude this introduction by a discussion about the expectation of the generated harmonic intensity as a function of propagation length. In the LP case, it is theoretically established by perturbation theory (which, however, limits the range of validity) [37] that the harmonic intensities scale quadratically as a function of the propagation distance due to cooperative phase matching. We shortly summarize here the corresponding physical process. For an x axis *linearly polarized* (LP) pulse of amplitude E_0, envelope $\mathcal{E}$, frequency ω_0, and wave number $k_0 = \omega_0/c$, propagating in the direction $\mathbf{e}_z$, $\mathbf{E}(\mathbf{x},t) = E_0\mathcal{E}(\mathbf{x},t)e^{i(k_0 z-\omega_0 t)}\mathbf{e}_x$, where $\mathbf{x} = (x,y,z)^T$, Maxwell's equations for $\mathbf{E}$ read

$$\partial_{tt}\mathbf{E} - c^2\triangle\mathbf{E} = -4\pi\,\partial_{tt}(\mathbf{P}_L + \mathbf{P}_{NL}) - 4\pi\,\partial_t\mathbf{J}, \qquad (2)$$

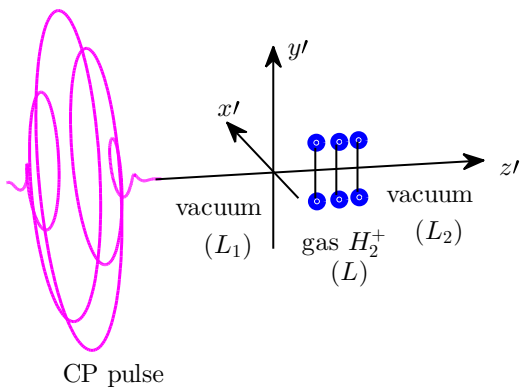

FIG. 1. Geometry of HHG from an incident circularly polarized pulse on aligned $H_2{}^+$ molecules.

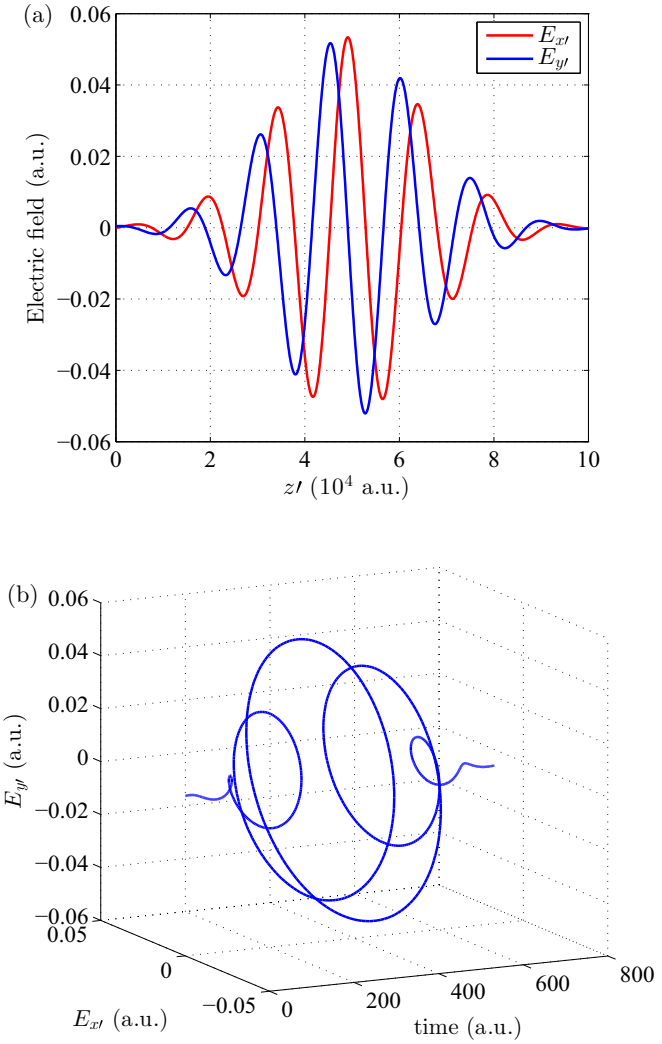

FIG. 2. (a) $E_{x'}$, $E_{y'}$ amplitudes of circularly polarized initial pulse in space for $I = 10^{14}$ W/cm^2, $\lambda_0 = 800$ nm, z'(a.u.) $= a_0 = 0.0529$ nm. (b) Total pulse in time; E(a.u.) $= 5\times10^9$ V/cm, time (a.u.) $=$ 24 as.

where $\mathbf{J}$ is the current density, $\mathbf{P}_L$ and $\mathbf{P}_{NL}$ are the linear and nonlinear polarization, such that the Fourier transform of $\mathbf{P}_{NL}$ satisfies $\widehat{\mathbf{P}}_{NL}(\mathbf{x},\omega) = \sum_{i=1}^{\infty}\widehat{\mathbf{P}}^{(2i+1)}(\mathbf{x},\omega)$, where to first order

$$\widehat{\mathbf{P}}_L(\mathbf{x},\omega) = \chi^{(1)}(\omega)\widehat{\mathbf{E}}(\mathbf{x},\omega), \qquad (3)$$

and in higher orders,

$$\begin{aligned}\widehat{\mathbf{P}}_{NL}^{(2i+1)}(\mathbf{x},\omega) = \int\int\cdots\int \chi^{(2i+1)}(\omega;\omega_1,\omega_2,\ldots,\omega_{2i+1})\\ \times\widehat{\mathbf{E}}(\mathbf{x},\omega_1)\widehat{\mathbf{E}}(\mathbf{x},\omega_2)\cdots\widehat{\mathbf{E}}(\mathbf{x},\omega_{2i+1})\\ \times\delta(\omega_1+\omega_2+\cdots+\omega_{2i+1}-\omega)\\ \times d\omega_1 d\omega_2\cdots d\omega_{2i+1}, \qquad (4)\end{aligned}$$

$\chi^{(2i+1)}$ is a rank $(2i+2)$ tensor of the medium susceptibility, while the factor $\delta(\omega_1+\omega_2+\cdots+\omega_{2i+1}-\omega)$ takes into account the energy-conservation law. This expansion is possible

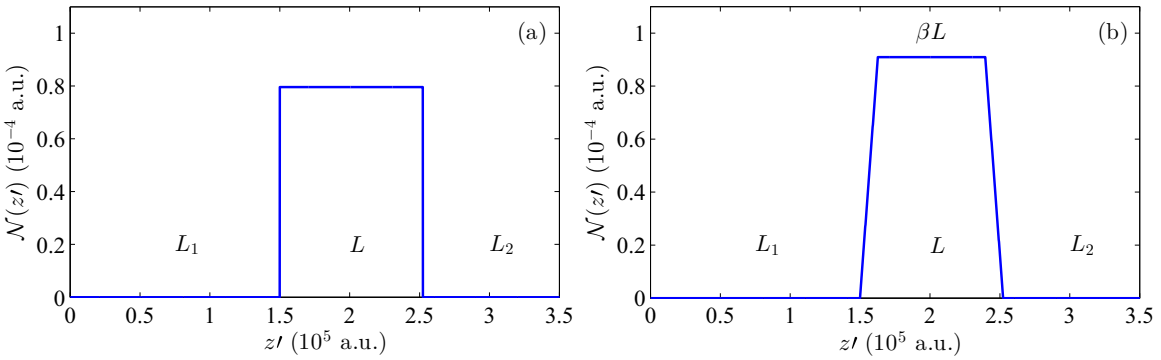

FIG. 3. (a) Homogeneous and (b) nonhomogeneous density profiles, $\mathcal{N}(z')$; $\mathcal{N}_0 = 8\times10^{-5}\ a_0^{-3}$.

by solving the laser-quantum particle TDSE by perturbation theory. The nonlinear refraction index n then reads $n = n_0 + n_2 I + n_4 I^2 + \cdots$, where I is the field intensity. In general, the nonlinearities introduce focusing and filamentation [1]. The above equations apply to linear polarization. We establish in this paper that, based on numerical experiments, the low-order odd-harmonic intensities scale quadratically with distance, when a CP probe pulse propagates in a H_2^+ molecule gas (centrosymmetric medium) and that the generated photons exhibit in the HHG process circular polarization (CP).

II. MAXWELL TIME-DEPENDENT SCHRÖDINGER-EQUATION MODEL

We study the process of attosecond pulse generation by the analysis of harmonic phases and intensities by using the micro-macro Maxwell–Schrödinger model, which consists of the coupling of Maxwell's equations (MEs) and TDSEs within or beyond the Born–Oppenheimer approximation. The model is totally nonperturbative, vectorial, and multidimensional, taking into account ionization and high-order nonlinearities beyond classical and semiclassical nonlinear Maxwell and Schrödinger models [38–40]. The MASP equations in the general case read

$$\begin{aligned}
\partial_t \mathbf{B}(\mathbf{x}',t) &= -c\boldsymbol{\nabla}\times\mathbf{E}(\mathbf{x}',t),\\
\partial_t \mathbf{E}(\mathbf{x}',t) &= c\boldsymbol{\nabla}\times\mathbf{B}(\mathbf{x}',t)\\
&\quad -4\pi[\partial_t\mathbf{P}(\mathbf{x}',t)+\mathbf{J}(\mathbf{x}',t)],\\
\boldsymbol{\nabla}\cdot\mathbf{B}(\mathbf{x}',t) &= 0,\\
\boldsymbol{\nabla}\cdot[\mathbf{E}(\mathbf{x}',t)+4\pi\mathbf{P}(\mathbf{x}',t)] &= 4\pi\left(\sum_{q=1}^{2} q\mathcal{N}_q(\mathbf{x}',t)-\mathcal{N}_e(\mathbf{x}',t)\right),
\end{aligned} \tag{5}$$

where $\mathcal{N}_q(\mathbf{x}',t)$ and $\mathcal{N}_e(\mathbf{x}',t)$ represent the number density of the ions with charge q ($q = 1,2$) and electrons, respectively. The initial ionic molecule density is taken to be continuous in space and is denoted by $\mathcal{N}(\mathbf{x}')$. It must be approximately equal to the initial electron number density $\mathcal{N}_e(\mathbf{x}')$. The polarization

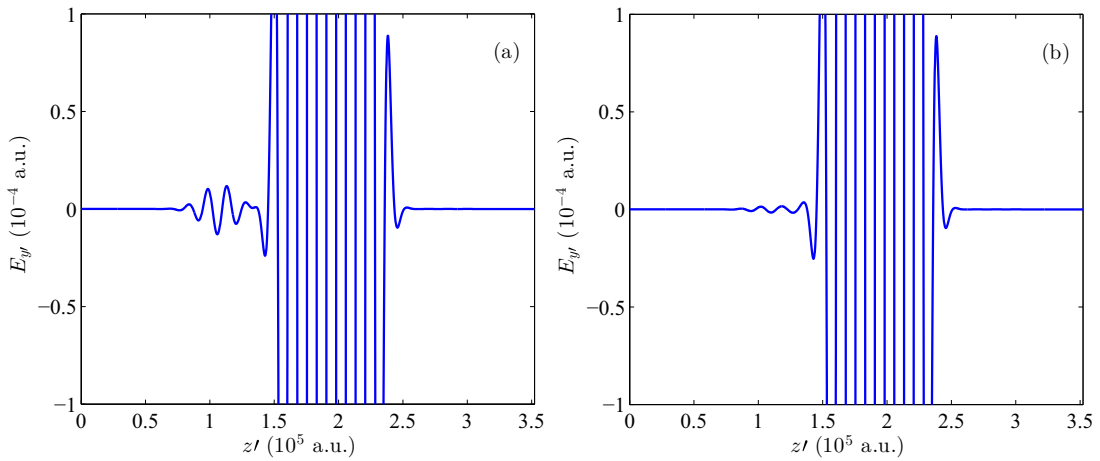

FIG. 4. (a) Reflection of E_y component at the entering border "vacuum-gas," $t = 722$ a.u., homogeneous case. (b) Reflection of E_y component at the entering border "vacuum-gas," $t = 722$ a.u., nonhomogeneous case with $\beta = 3/4$, time (a.u.) = 24 as.

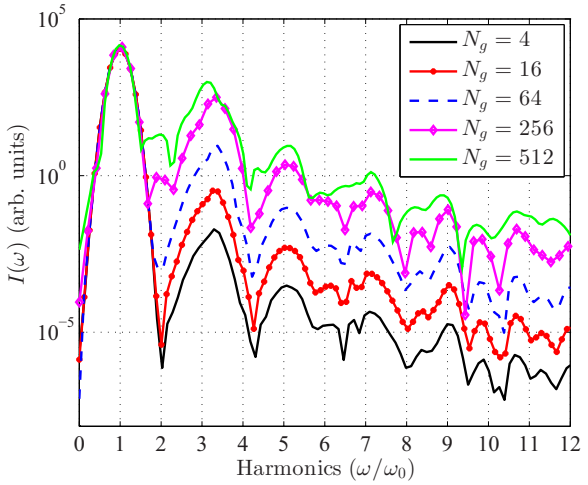

FIG. 5. Intensity of the low-order electric-field harmonic spectrum for different gas-region lengths $L = \Delta z_M N_g$ for LP pulses ($\lambda = 800$ nm, $I = 5\times10^{13}$ W/cm^2, $\Delta z_M = 100$ a.u.).

is obtained from the TDSE

$$\mathbf{P}(\mathbf{x}',\mathbf{t}) = \mathcal{N}(\mathbf{x}')\sum_{i=1}^{m}\mathbf{d}_i(\mathbf{x}',t)$$
$$= -\mathcal{N}(\mathbf{x}')\sum_{i=1}^{m}\chi_{\Omega_i}(\mathbf{x}')\int_{\mathbb{R}^3}\psi_i(\mathbf{x},t)\mathbf{x}\psi_i^*(\mathbf{x},t)d\mathbf{x},$$

$$i\partial_t\psi_i(\mathbf{x},t) = -\frac{1}{2}\Delta_{\mathbf{x}}\psi_i(\mathbf{x},t) + V_c(\mathbf{x})\psi_i(\mathbf{x},t)$$
$$+\mathbf{x}\cdot\mathbf{E}_{\mathbf{x}_i'}(t)\psi_i(\mathbf{x},t),\ \forall\, i\in\{1,\dots,m\}, \qquad (6)$$

where V_c denotes the nuclear Coulomb potential and $\mathbf{x}' = (x',y',z')^T$ denotes the electromagnetic field space variables and for the Born–Oppenheimer approximation, the TDSE space variables are $\mathbf{x} = (x,y,z)^T$. In the $1-d/2-$d model which is considered in this paper, two-dimensional H_2^+

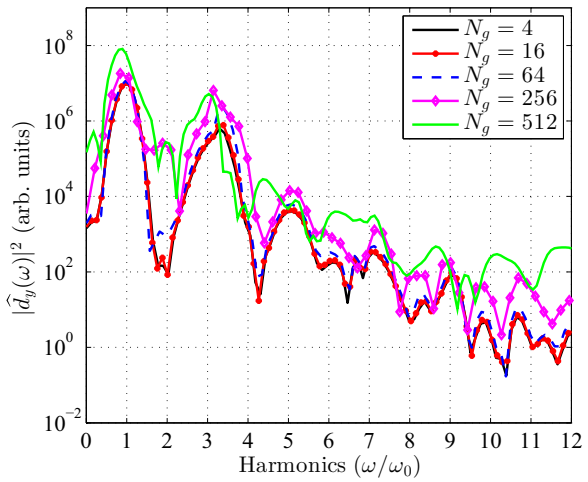

FIG. 6. Intensity of harmonics of the dipole moment $\widehat{d}_y(\omega)$ of molecule in the right end of gas region for different propagation lengths $L = \Delta z_M N_g$ of LP pulses ($\lambda = 800$ nm, $I = 5\times10^{13}$ W/cm^2, $\Delta z_M = 100$ a.u.).

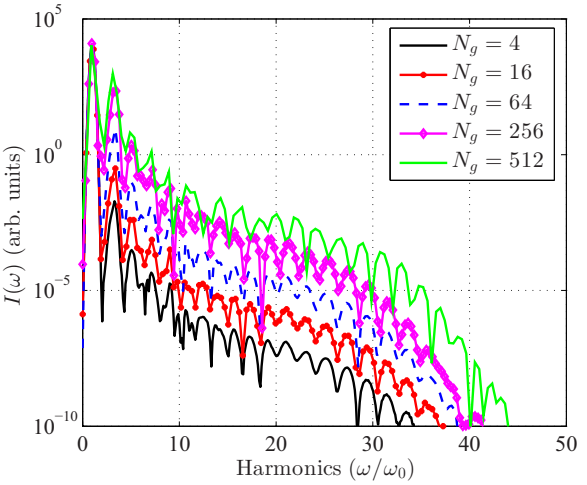

FIG. 7. Intensity of harmonics of the transmitted electric field for different gas-region lengths $L = \Delta z_M N_g$ for LP pulses.

molecules are aligned in the z direction, oriented in the y direction, and are subjected to the circularly polarized electric field $\mathbf{E}(\mathbf{x}',t)$ propagating in the direction z. The electric field first propagates in vacuum, then in the gas, and finally exits in vacuum; see Fig. 1. The two-dimensional (2-d) electron wave function $\psi_{z'}$ in Eq. (6) is solved by the following TDSE modeling a molecule "located at z'":

$$i\partial_t\psi_{z'}(x,y,t) = \big(-\tfrac{1}{2}\triangle + V_c(x,y,R_0)$$
$$+xE_{x,z'}(t) + yE_{y,z'}(t)\big)\psi_{z'}(x,y,t). \qquad (7)$$

In Eq. (7), R_0 denotes the molecular internuclear distance, z' is the field propagation coordinate, and (x,y) is the electric-field polarization corresponding to the electron coordinates. The molecular polarization is calculated as

$$\mathbf{P}(z',t) = -\mathcal{N}(z')\int\psi_{z'}(x,y,t)\mathbf{x}\psi_{z'}^*(x,y,t)dxdy$$
$$= \mathcal{N}(z')\mathbf{d}_{z'}(t). \qquad (8)$$

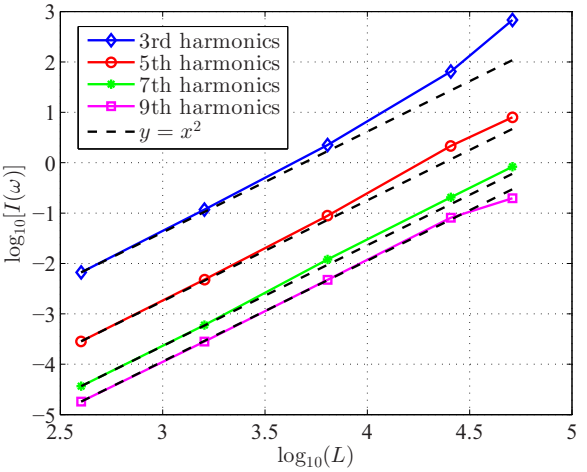

FIG. 8. Intensity of the low-order harmonics as a function of the propagation length $L = \Delta z_M N_g$ of the LP pulse.

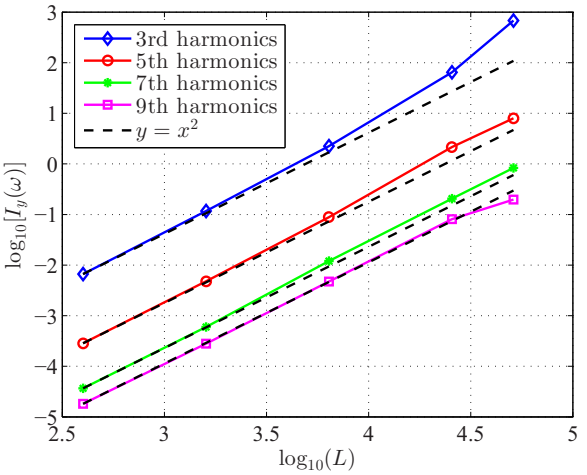

FIG. 9. Intensity of the low-order harmonics of the electric E_y component as a function of propagation length $L = \Delta z_M N_g$ of the LP pulse in gas.

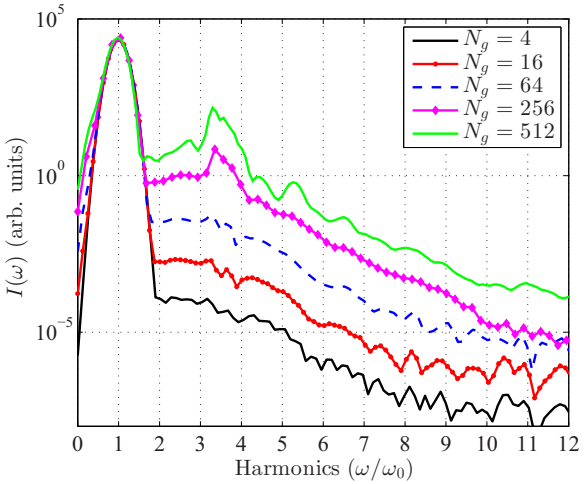

FIG. 10. Low-order harmonic spectrum of the transmitted electric field for different gas-region lengths $L = \Delta z_M N_g$ for a CP pulse.

with density $\mathcal{N}(z')$. In the following, we denote by $\mathbf{E}$ the electric field (E_x, E_y), and by $\mathbf{P} = (P_x, P_y)$ the field-induced polarization computed from the field-induced dipole moment $\mathbf{d}_{z'}$. Under the dipole approximation in the x, y directions, the electric field depends on z', and $\mathbf{E}(z',t)$ is denoted by $\mathbf{E}_{z'}(t)$. Alternatively to the dipole moment, one can use the acceleration of the electron as given in Ref. [20] [Fourier transform $\widehat{\mathbf{a}}_{z'}(\omega) = \omega^2 \widehat{\mathbf{d}}_{z'}(\omega)$]:

$$\mathbf{a}_{z'}(t) = \int \psi_{z'}(x,y,t)[-\nabla V_c(x,y,R_0) + \mathbf{E}_{z'}(t)] \times \psi^*_{z'}(x,y,t)dxdy. \quad (9)$$

The MASP model is solved by using a finite-difference method described in detail in Ref. [5].

III. APPLICATION OF THE MAXWELL–SCHRÖDINGER-PLASMA MODEL

As illustrated in Fig. 1, the laser pulse propagates in the z' direction through a vacuum region (of length L_1), then in a $H_2{}^+$-gas region (of length L), and finally in a vacuum region (of length L_2). The x', y' components of the circularly polarized (CP) field $\mathbf{E}(\mathbf{x}',t)$ and $\mathbf{B}(\mathbf{x}',t)$ are functions of the z' coordinate and time only in the (x,y) dipole approximation:

$$\mathbf{E}(\mathbf{x}',\mathbf{t}) = (E_{x'}(z',t), E_{y'}(z',t)),$$
$$\mathbf{B}(\mathbf{x}',t) = (B_{x'}(z',t), B_{y'}(z',t)), \quad (10)$$

TABLE I. Propagation time and L^2 norm of the wave function after impact of the laser pulse.

N_g	Final time (a.u.)	$\|\psi\|^2_{L^2}$ (LP)	$\|\psi\|^2_{L^2}$ (CP)
4	869.815	0.972 799	0.952 074
16	878.485	0.973 138	0.949 644
64	913.162	0.972 781	0.949 84
256	1051.87	0.972 088	0.947 415
512	1236.81	0.971 847	0.945 787

so that the MEs (6) become

$$\partial_t E_{x'}(z',t) = -c\partial_{z'} B_{y'}(z',t) - 4\pi \partial_t P_{x'}(z',t),$$
$$\partial_t E_{y'}(z',t) = c\partial_{z'} B_{x'}(z',t) - 4\pi \partial_t P_{y'}(z',t),$$
$$\partial_t B_{x'}(z',t) = c\partial_{z'} E_{y'}(z',t),$$
$$\partial_t B_{y'}(z',t) = -c\partial_{z'} E_{x'}(z',t). \quad (11)$$

The initial circularly polarized (CP) ultrashort laser pulse is chosen in vacuum in the form (we note that the dipole approximation is applied in the polarization plane x', y', but not in the propagation direction z')

$$E_{x'}(z',t) = E_{0x'} f(k_0 z' - \omega_0 t)\sin(k_0 z' - \omega_0 t),$$
$$E_{y'}(z',t) = E_{0y'} f(k_0 z' - \omega_0 t)\cos(k_0 z' - \omega_0 t),$$
$$B_{x'}(z',t) = -B_{0x'} f(k_0 z' - \omega_0 t)\cos(k_0 z' - \omega_0 t),$$
$$B_{y'}(z',t) = B_{0y'} f(k_0 z' - \omega_0 t)\sin(k_0 z' - \omega_0 t), \quad (12)$$

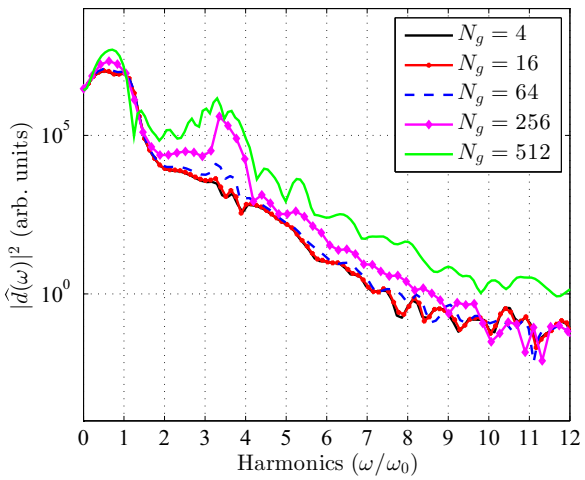

FIG. 11. Low-order harmonic of the dipole moment of aligned $H_2{}^+$ molecules in the right (exit) end of the gas region for different propagation lengths $L = \Delta z_M N_g$ of CP pulses.

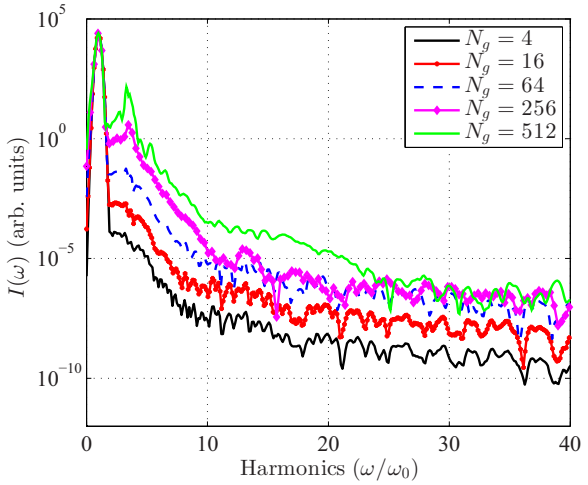

FIG. 12. Total harmonic spectrum of the transmitted electric field for different gas-region lengths $L = \Delta z_M N_g$ for a CP pulse.

where ω_0 is the central frequency, $k_0 = \omega_0/c = 2\pi/\lambda_0$ is the corresponding wave number, which in the simulations we take to be $\lambda_0 = 800$ nm, $\omega_0 \simeq 0.057$ a.u.

In the case of CP pulses the field amplitudes can be written as a function of the pulse intensity I as follows: $E_{0x'} = E_{0y'} = B_{0x'} = B_{0y'} = \sqrt{8\pi I/c}$, whereas for linearly polarized (LP) pulses we have $E_{0y'} = B_{0x'} = \sqrt{8\pi I/c}$. In the computations $I = 10^{14}$ W/cm^2 $= 2.84\times10^{-3}$ a.u. [I(a.u.) $= 3.5\times10^{16}$ W/cm^2].

In Eq. (12), the function f is the envelope of the initial electromagnetic field, which in our computations is chosen as a Gaussian [see Figs. 2(a) and 2(b)], $f(k_0 z' - \omega_0 t) = e^{-\alpha(k_0 z' - \omega_0 t)^2}$ with $\alpha = 3\times10^{-9}$, and the phase $(k_0 z' - \omega_0 t)$ is expressed in a.u. ($k_0 = \omega/c \approx 0.057/137 \approx 4.16\times 10^{-4}$ a.u.).

The electromagnetic (EM) field (12) satisfies Maxwell's equations in vacuum, where in Eq. (11) $\partial_t P_{x'}(z',t) = \partial_t P_{y'}(z',t) = 0$, as well as $\nabla\cdot\mathbf{E} = 0$, $\nabla\cdot\mathbf{B} = 0$.

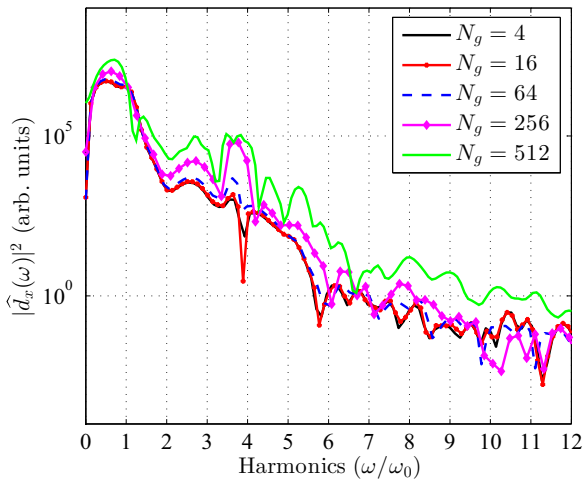

FIG. 13. Low-order harmonic spectrum of the dipole-moment component $d_x(\omega)$ of $H_2{}^+$ molecules in the right end of the gas region for different propagation lengths of CP pulses.

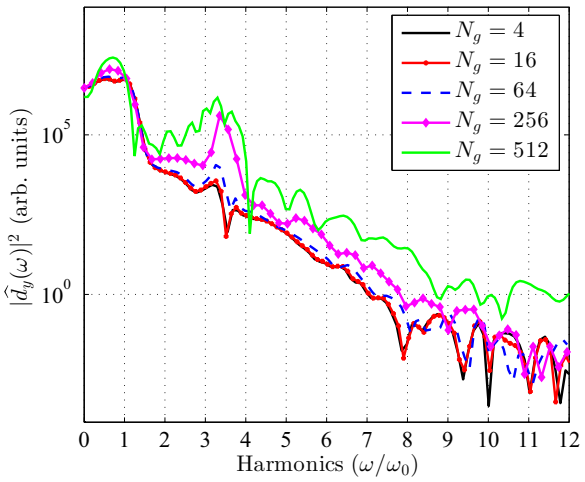

FIG. 14. Low-order harmonic spectrum of the dipole-moment component $d_y(\omega)$ of $H_2{}^+$ molecules in the right end of the gas region for different propagation lengths of CP pulses.

In such a geometry the molecular density in the second medium region (of length L) can be considered as a function of the z' coordinate only. Namely, in the current computations, two options were used: (a) homogeneous density (HD), where $\mathcal{N}(z') = \mathcal{N}_0$, and (b) nonhomogeneous, where

$$\mathcal{N}(z') = \begin{cases} \frac{(z'-L_1)}{L}\frac{4\mathcal{N}_0}{1-\beta^2}, & z' \in [L_1, L_1+L'] \\ \frac{2\mathcal{N}_0}{1+\beta}, & z' \in [L_1+L', L_1+L-L'] \\ \frac{(L_1+L-z')}{L}\frac{4\mathcal{N}_0}{1-\beta^2}, & z' \in [L_1+L-L', L_1+L], \end{cases} \tag{13}$$

chosen such that $\int_{L_1}^{L_1+L}\mathcal{N}(z')\Delta z_M = \mathcal{N}_0 L$, with $L' = \frac{1-\beta}{2}L$, where β is a positive coefficient less than unity; see Fig. 3.

The nonhomogeneous model is found to reduce or smooth out the EM-wave reflections at both interfaces between the gas and vacuum regions, as illustrated in Fig. 4 for the

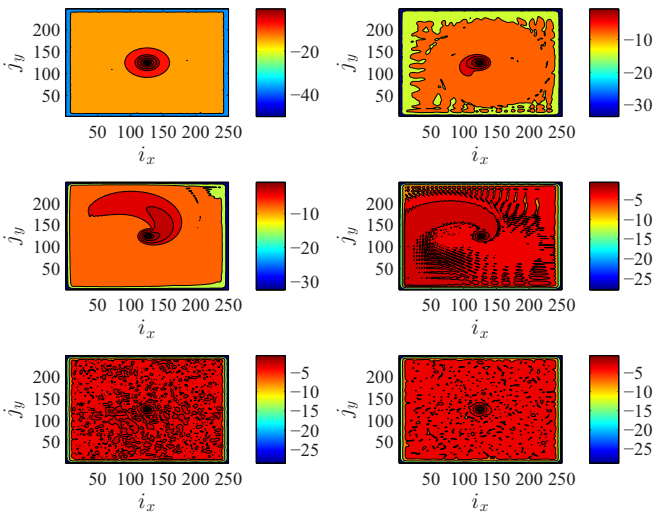

FIG. 15. The level sets of electron density $\log_{10}(|\psi(x,y)|^2)$ for a $H_2{}^+$ molecule in the left (entering) end of the gas region at six consecutive times: $t = 0$, 302, 349, 451, 757, 1237 a.u., time (a.u.) $= 24$ as. Total number of TDSEs is $N_g = 512$.

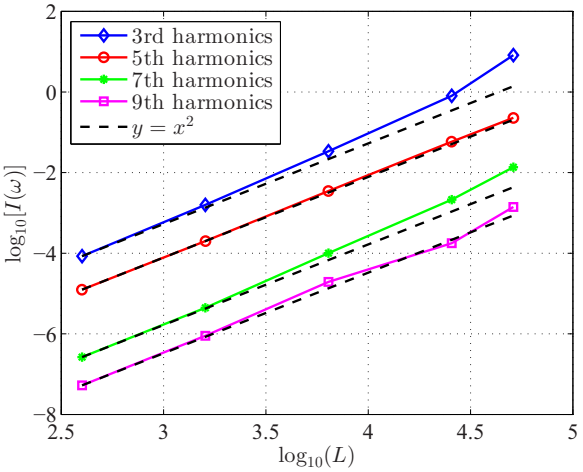

FIG. 16. Intensity of the low-order harmonics as a function of the propagation length $L = \Delta z_M N_g$ of the CP pulse in gas.

entering border case. In the reported further computations, we choose $\mathcal{N}_0 = 5.17\times10^{-5}\, a_0^{-3} \approx 3.5\times10^{20}$ mol/cm^3, corresponding to ≈13 atmospheres.

We next discuss the numerical approximation of the MASP model by the finite-difference scheme (FDS). Maxwell's equations are approximated by a second-order scheme with the Courant, Friedrichs, and Lewy (CFL) stability condition $c\Delta t_M/\Delta z_M \lesssim 1$, avoiding artificial diffusion, where Δt_M, Δz_M denote the time and space steps in the numerical scheme [41]. The vacuum and gas regions have lengths $L_1 = \Delta z_M N_1$, $L = \Delta z_M N_g$, and $L_2 = \Delta z_M N_2$, with spatial discretization $\Delta z_M = 100$ a.u. (≈5.29 nm), $N_1 = N_2 = 999$, while N_g, which is the number of cells along z' in the gas region, consequently takes the values 4, 16, 64, 256, and 512. Each Maxwell spatial step Δz_M is chosen such that $\Delta z_M < \lambda_0/5$ where $\lambda_0 = 800$ nm is the largest pulse wavelength considered in the computation.

As we solve one single TDSE per Maxwell cell of size Δz_M, a computation of N_g TDSEs corresponds to a sample of gas of length $L = N_g \Delta z_M$, which contains $N_g \Delta z_M \mathcal{N}_0$

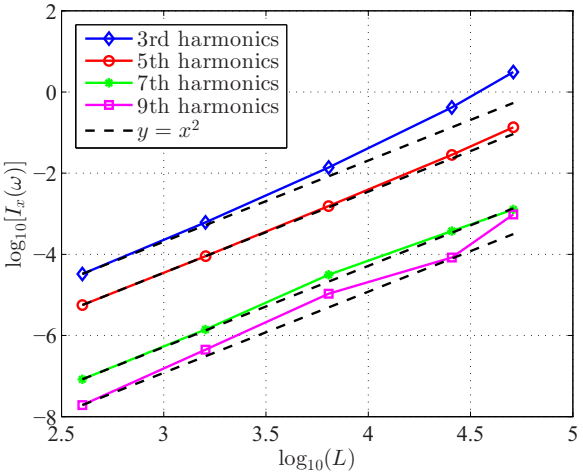

FIG. 17. Intensity of the low-order harmonics of the E_x component as a function of propagation length $L = \Delta z_M N_g$ of the CP pulse in gas.

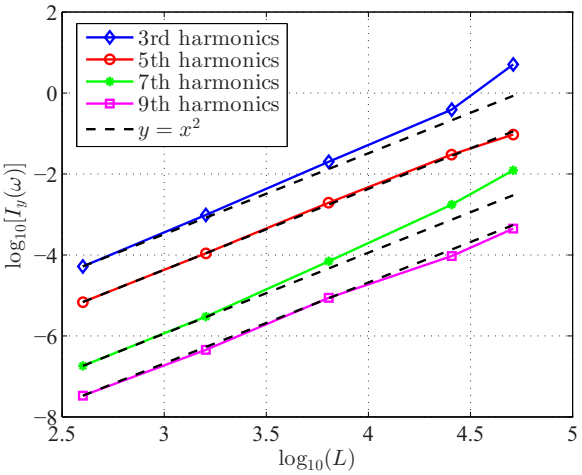

FIG. 18. Intensity of the low-order harmonics of the E_y component as a function of propagation length $L = \Delta z_M N_g$ of the CP pulse in gas.

molecules, when the molecular density $\mathcal{N}(z') = \mathcal{N}_0$ is supposed to be constant. TDSEs are solved by a Crank–Nicolson finite difference scheme (FDS) of second order, which is unconditionally stable and ℓ^2-norm preserving. The molecular $H_2{}^+$ TDSE spatial-temporal solver steps are denoted Δx_S, Δy_S, and Δt_S, which satisfy $\Delta t_M/\Delta t_S \gg 1$, $\Delta z_M/\Delta x_S \gg 1$, $\Delta z_M/\Delta y_S \gg 1$. In a.u., the $H_2{}^+$ TDSEs read

$$i\partial_t\psi(x,y,t) = -\tfrac{1}{2}\Delta_{x,y}\psi(x,y,t) + V_c(x,y,R_0)\psi(x,y,t) + [xE_{z',x}(t) + yE_{z',y}(t)]\psi(x,y,t). \quad (14)$$

Each equation is solved using a second-order Strang splitting in time:

$$\begin{aligned}
\partial_t\psi(x,y,t) &= -i[xE_{z',x}(t) + yE_{z',y}(t)]\psi(x,y,t),\\
&\quad t \in [t_n, t_{n+1/2}], \quad \psi(x,y,t_n) = \psi^n(x,y),\\
\partial_t\psi(x,y,t) &= \frac{i}{2}\Delta_{x,y}\psi(x,y,t) - iV_c(x,y,R_0)\psi(x,y,t),\\
&\quad t \in [t_n, t_{n^*+1}], \quad \psi(x,y,t_n) = \psi^{n+1/2}(x,y),\\
\partial_t\psi(x,y,t) &= -i[xE_{z',x}(t) + yE_{z',y}(t)]\psi(x,y,t),\\
&\quad t \in [t_{n+1/2}, t_{n+1}], \quad \psi\left(x,y,t_{n+1/2}\right) = \psi^{n^*+1}(x,y).
\end{aligned} \quad (15)$$

We have denoted by ψ^n, $\psi^{n+1/2}$ the space-dependent wave function at time t_n, $t_{n+1/2}$. The first step provides $\psi^{n+1/2} = \psi^n \exp[-i(xE^n_{z',x} + yE^n_{z',y})\Delta t_S/2]$, where $\Delta t_S = t_{n+1} - t_n = t_{n^*+1} - t_n = 2(t_{n+1} - t_{n+1/2}) = 2(t_{n+1/2} - t_n)$. In the second step, the corresponding laser-free TDSE with initial data $\psi^{n+1/2}$ is numerically solved and, finally, the third step is solved as the first one: $\psi^{n+1} = \psi^{n^*+1} \exp[-i(xE^{n+1/2}_{z',x} + yE^{n+1/2}_{z',y})\Delta t_S/2]$.

In the second step, we solve the 2-d TDSE with absorbing boundary conditions in order to eliminate electron artificial

reflection in each TDSE domain, Ω,

$$\begin{aligned}\partial_t\psi(x,y,t) &= \frac{i}{2}\Delta_{x,y}\psi(x,y,t) - iV_c(x,y,R_0)\psi(x,y,t),\\ &(x,y)\in\Omega,\quad t>0,\\ \psi(x,y,0) &= \psi_0(x,y),\quad (x,y)\in\Omega,\\ \psi(x,y,t) &= 0,\quad (x,y)\in\Gamma:=\partial\Omega,\quad t>0,\end{aligned}\tag{16}$$

where $\Omega=(a,b)\times(c,d)$ and $d-c=b-a=60$ (or 90) a.u.

In our computations $\Delta x_S=\Delta y_S=0.3$ a.u. with 200 (or 500) grid points in each direction. Such discretization establishes maximum free electron momentum $p_x=p_y=\pi/\Delta x_S\approx 10$ a.u. or equivalently a maximum energy $\mathcal{E}=p^2/2$ a.u. ≈ 100 a.u. ≈ 2700 eV. In Eq. (16) the nuclear potential of $H_2{}^+$ is written as (in a.u.)

$$\begin{aligned}&V_c(x,y,R_0)\\ &=-\left[\left(x-\frac{R_0}{2}\cos\theta\right)^2+\left(y-\frac{R_0}{2}\sin\theta\right)^2+\varepsilon\right]^{-1/2}\\ &\quad-\left[\left(x+\frac{R_0}{2}\cos\theta\right)^2+\left(y+\frac{R_0}{2}\sin\theta\right)^2+\varepsilon\right]^{-1/2},\end{aligned}\tag{17}$$

where $\theta\in[0^\circ,90^\circ]$ defines the angle between the molecular axis of $H_2{}^+$ and the x axis, with $R_0=2$ a.u. being the internuclear distance. The value of $\varepsilon=4.5$ is used to reproduce the computational energy of the ground state of $H_2{}^+$-molecule ≈ -0.58 a.u. The time step for solving the TDSEs is chosen as $\Delta t_S=\Delta t_M/20\approx 0.036$ a.u. (1 a.u. $\approx$ 24 as).

The parallel-computing strategy described in Ref. [42] is used for solving the large set of 2-d TDSEs. More specifically, on p processors, the gas region is decomposed in p subdomains, containing $S\in\mathbb{N}^*$ Maxwell cells in which we solve one TDSE, and from which we deduce the local macroscopic polarization (6). At each TDSE time iteration, each processor solves sequentially S TDSEs, with a total of pS TDSEs modeling the gas. The time step for solving MEs is $\Delta t_M=\mathrm{CFL}\Delta z_M/c\approx 0.722$ a.u. with $\mathrm{CFL}=0.99$, see Ref. [41]. We neglect the interaction between $H_2{}^+$ molecules, because at pressure of 13 atmospheres ($\mathcal{N}_0=5.17\times10^{-5}a_0^{-3}$) the average distance between $H_2{}^+$ molecules is $27a_0$ (1.4 nm) which exceeds largely the molecular dimension $R_0=2$ a.u.

IV. PHYSICAL RESULTS

A. Linearly polarized pulse

We first study the propagation of LP laser pulses in the $H_2{}^+$ gas modeled by 2-d TDSEs. The initial laser pulse is chosen as follows: $E_x=0$, $B_y=0$, with E_y and B_x defined in Eq. (12), at the intensity $I_y=5\times10^{13}$ W/cm$^2=1.42\times10^{-3}$ a.u. $H_2{}^+$ molecules are oriented along the y axis (i.e., parallel to E_y, see Fig. 1). In the following simulation the gas density is assumed constant in space and time. The computation grid for the TDSEs is a 200×200-point grid. In Fig. 5, we report the harmonic spectrum up to the 11th harmonic of the intensity of the electric field, $I(\omega)=I_x(\omega)+I_y(\omega)\propto|\widehat{E}_x(\omega)|^2+|\widehat{E}_y(\omega)|^2$, as a function of the propagation length of the LP pulse. Notice that, in the case of the initial LP pulse $I_x(\omega)\ll I_y(\omega)$, i.e., "$(\omega,I(\omega))\approx(\omega,I_y(\omega))$". In Fig. 6, we report the harmonic spectrum (in the same interval, i.e., up to the 11th harmonic) of the y component of the dipole

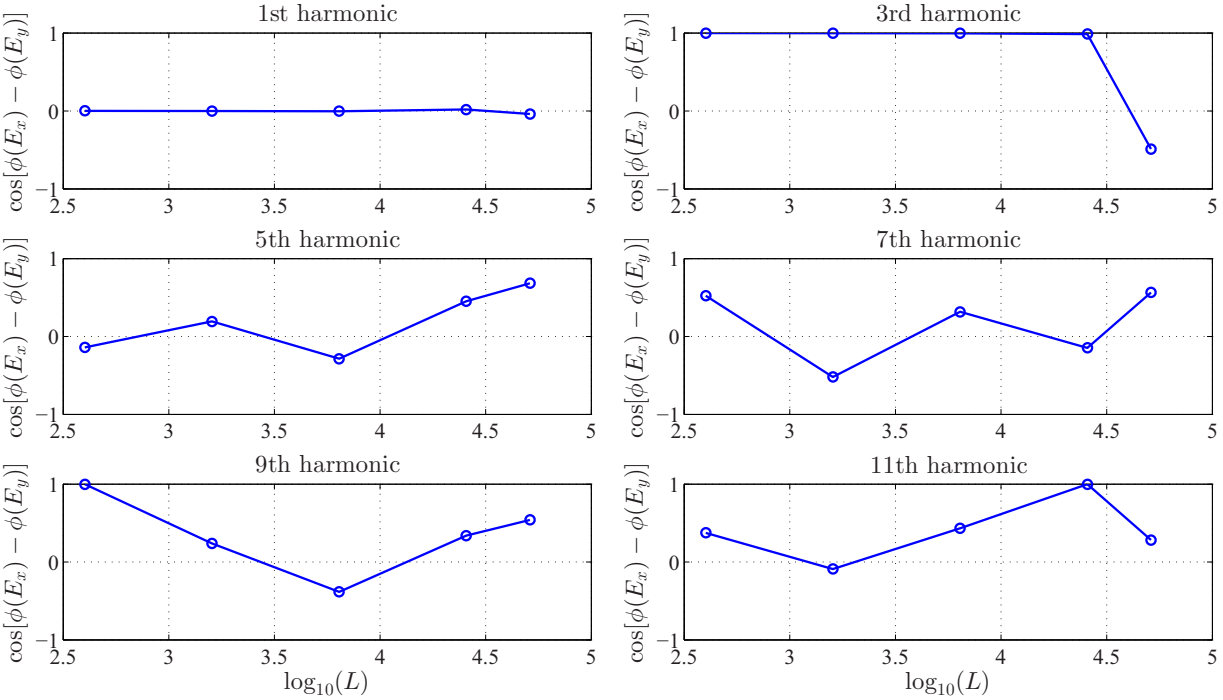

FIG. 19. $\cos(\phi\{\widehat{E}_x[(2k+1)\omega_0]\}-\phi\{\widehat{E}_y[(2k+1)\omega_0]\})$, for $k=0,1,2,3,4,5$ as a function of propagation length $L=\Delta z_M N_g$ of the CP pulse. Circularly polarized harmonics are generated at zero corresponding to a $\pm\pi/2$ phase difference.

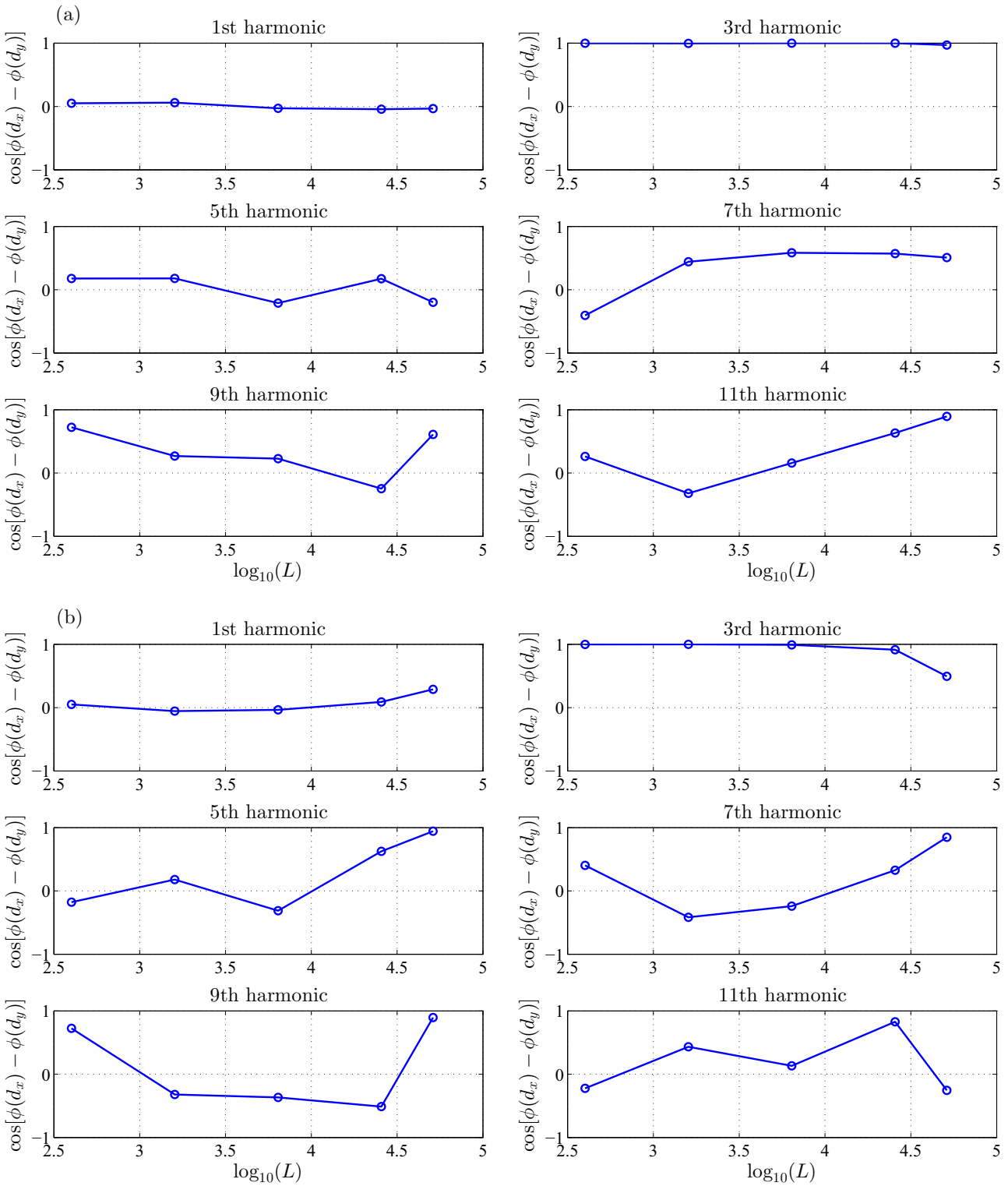

FIG. 20. $\cos(\phi\{\widehat{d}_x[(2k+1)\omega_0]\} - \phi\{\widehat{d}_y[(2k+1)\omega_0]\})$, for $k = 0, 1, 2, 3, 4, 5$ as a function of propagation length $L = \Delta z_M N_g$ of the CP pulse, for H_2^+ molecules at the (a) left end (incident) and (b) at the right-end (outgoing) of the gas region.

moment d_y, $(\omega, |\widehat{d}_y(\omega)|^2)$, of a molecule located at the right end of the gas region, for different "gas-region lengths." Figure 7 also illustrates the whole spectrum $(\omega, I(\omega))$ up to the cutoff region about the 30th harmonic. In Figs. 8 and 9, we report the intensities, $I(\omega)$, $I_y(\omega)$ of the first generated odd harmonics (3,5,7,9) on a log scale and as a function of the propagation length. These results are consistent with those of Ref. [30], where the quadratic scaling harmonic intensities and/or propagation length, was observed in a 1-d/1-d model.

B. Circularly polarized pulse

The initial CP pulse (12) has a total intensity $I = 10^{14}$ W/cm^2, i.e., 5×10^{13} W/cm^2 per component of the electric field, E_x and E_y. The H_2^+ nuclei lie along the y axis. Since the CP-electron radius becomes $r(E) = 3.7E_0/\omega^2 \approx 44$ a.u. [43], the TDSE grid is now a 500×500-point grid or 150×150 a_0^2. In Table I, we report the propagation time, as well as the L^2-norm of the wave function "after the pulse"—both LP and CP cases for comparison. All the results in the table and on the following graphs refer to the case of homogeneous density, except when nonhomogeneous density is explicitly specified.

In Fig. 10, we report the electric-field harmonic spectrum intensity (first 11 harmonics) $I(\omega)$ as a function of propagation length of the CP pulse in the gas. In Fig. 11, we report the harmonic spectrum of the squared absolute value of the dipole moment [see Eq. (8)] $(\omega, |\widehat{d}(\omega)|^2)$ of a molecule located in the right boundary of the gas region, for different gas-region lengths. In Fig. 12, we show the same spectrum up to the 40th harmonic. In Figs. 13 and 14, the harmonics spectra $(\omega, |\widehat{d}_x(\omega)|^2)$ and $(\omega, |\widehat{d}_y(\omega)|^2)$ are shown separately.

In Fig. 15, we report the temporal evolution of the squared absolute value of the wave function of a molecule in the left end of the gas region. In order to avoid spurious reflections at the computational domain boundary, we impose absorbing boundary conditions with artificial potential $U_{\text{abs}} = -V_1(x,y) - iV_2(x,y)$, such that the positive definite functions V_1 and V_2 are decreasing linearly in x or y while approaching the edges of the computational domain, defined by a 500×500-point grid.

In Figs. 16–18, we report the intensity $I(\omega)$, $I_x(\omega)$, and $I_y(\omega)$, of the first generated odd harmonics (3rd, 5th, 7th, 9th) on a log scale, as a function of the propagation length of the CP pulse in the gas. These results suggest that the quadratic scaling (intensity and/or propagation length) which was observed and justified in the LP case is also satisfied in the CP case for the first odd harmonics. Indeed, in a gas the influence of E_y on P_x through wave function [see Eqs. (6) or (7)] is negligible with respect to the influence E_x on P_x (the same can be said about E_x and P_y). On the other hand, the system (11) for CP pulses contains two independent wave equations: for E_x and E_y (if one excludes B_y and B_x, respectively). Each of these equations can be simplified by using the SVEA, which in the perturbative regime results in $I_x(\omega) \sim L^2$ and $I_y(\omega) \sim L^2$ independently.

The above results illustrate that high-frequency photons are coherently in the CP case to generate coherent shorter pulses than the probe pulse. We analyze further the harmonic phases $\phi_x[(2k+1)\omega_0] := \text{Arg}\{\widehat{E}_x[(2k+1)\omega_0]\}$, $\phi_y[(2k+1)\omega_0] := \text{Arg}\{\widehat{E}_y[(2k+1)\omega_0]\}$, for $k \in \mathbb{N}$. More specifically, the condition $\widehat{E}_y[(2k+1)\omega_0]/\widehat{E}_x[(2k+1)\omega_0] = \exp(i\{\phi_y[(2k+1)\omega_0] - \phi_x[(2k+1)\omega_0]\}) = \pm i$ must be satisfied, which corresponds to a $\pi/2$ phase difference between E_x and E_y. Figure 19 reports $\cos(\phi_x - \phi_y)$ for the 1st, 3rd, 5th, 7th, 9th, and 11th electric field harmonics as a function of the propagation length. The $\cos(\phi_x - \phi_y) = 0$ condition is observed numerically, thus confirming CP harmonics. In contrast, the phase differences of the 5th and 9th harmonics differ somewhat from the zero condition.

In Fig. 20, we report the cosinus of the dipole phase difference of $\widehat{d}_x[(2k+1)\omega_0]$ and $\widehat{d}_y[(2k+1)\omega_0]$ at $k = 1, 2, 3, 4, 5$ as a function of the propagation length, for a molecule located at the left-end (incident) region and a molecule located at the right end (outgoing) of the gas region; that is, $\cos\{\nu_x[(2k+1)\omega_0] - \nu_y[(2k+1)\omega_0]\}$, where $\nu_x[(2k+1)\omega_0] := \text{Arg}\{\widehat{d}_x[2(k+1)\omega_0]\}$ and $\nu_y[(2k+1)\omega_0] := \text{Arg}\{\widehat{d}_y[2(k+1)\omega_0]\}$. When this value is close to 0, as in the case of the 5th and 9th harmonics, we conclude to the emission of circularly polarized photons of frequency $2(k+1)\omega_0$.

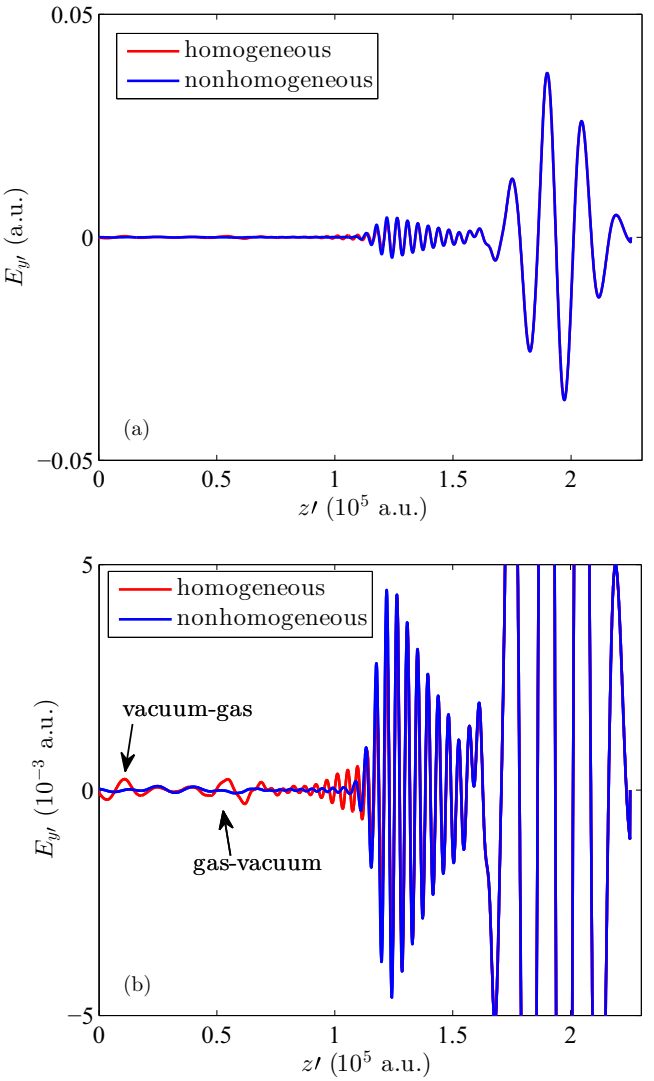

FIG. 21. (a) E_y as a function of space at final time with homogeneous and nonhomogeneous [$\beta = 1/3$ in Eq. (13)], molecular density. (b) Same figure with zoom along y.

We also report the electric field E_y components in real space, at final time $t = 1051.87$ a.u. ≈ 25 fs, modeled by 256 TDSEs, with homogeneous and nonhomogeneous (Fig. 3) molecule density. The difference between these two configurations is rather small and is illustrated in Fig. 21(a) and magnified in Fig. 21(b). As expected, the nonhomogeneous density allows for a reduction of the reflection of the incoming pulse at the gas-region boundaries (both vacuum-gas and gas-vacuum boundaries). The pulse propagating through an interface where the density varies from 0 to $\mathcal{N}_0$ is largely

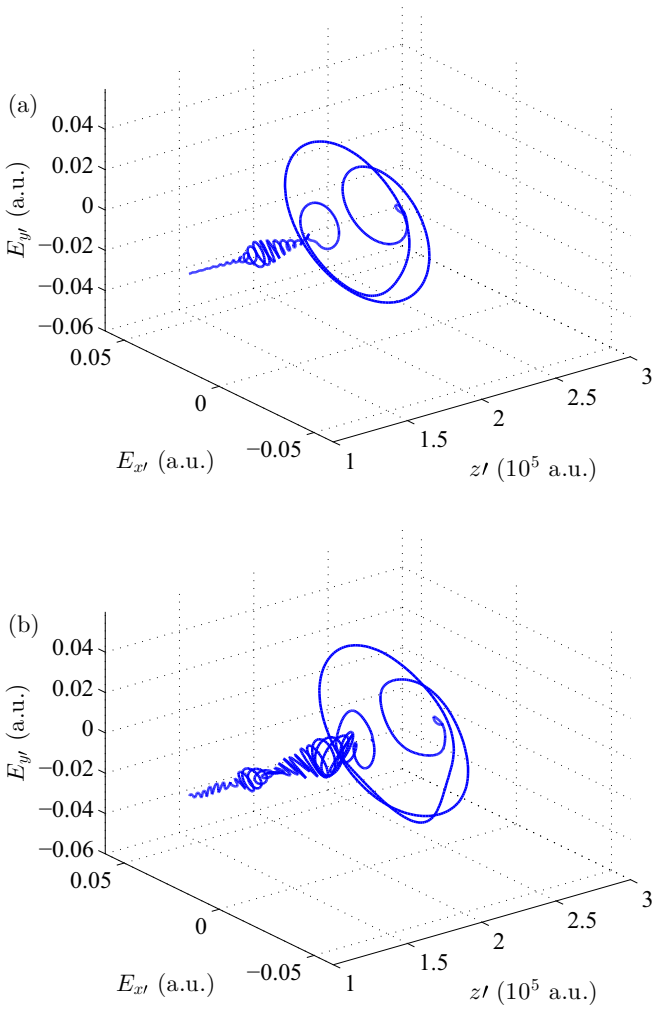

FIG. 22. Transmitted electric field as a function of space at final time with homogeneous molecular density. (a) $N_g = 256$. (b) $N_g = 512$.

reflected. In the nonhomogeneous case the density smoothly varies from 0 to $2\mathcal{N}_0/(1+\beta)$, and we observe that the reflected wave is of much smaller amplitude. However, small-amplitude high-frequency waves exist for both cases, homogeneous and nonhomogeneous, and seem unrelated to wave reflection.

In Fig. 22, we report the electric field **E** modeled by 256 [Fig. 22(a)] and 512 [Fig. 22(b)] TDSEs, with homogeneous molecule density in the (x,y) space. While the upper pulse visually demonstrates CP configuration, the structure of the propagating pulse in the case of $N_g = 512$ is strongly perturbed by the gas, and the circular polarization only is suppressed.

V. CONCLUSION

In this paper we study the generation of circularly polarized harmonics and propagation effects in a 2-d H_2^+ gas. As discussed in Refs. [2,44], more complex molecules like O_2 and N_2 could also be considered by using the single-active-electron approximation [45]. Numerical simulations of a MASP model allows for a nonperturbative calculation of the macroscopic polarization in Maxwell's equations using the solution of H_2^+ molecular TDSEs under the influence of an intense laser pulse. The MASP model permits the accurate observation of the generation of high harmonics and nonlinearities through multiphoton ionization, as well as the inclusion of corresponding coherent effects at the macroscopic scale. Although it is theoretically possible to rigorously derive the macroscopic nonlinear polarization from laser-molecule TDSEs in the case of linearly polarized pulses, the circularly polarized case is more complex. Through the numerical MASP model, we have obtained the dipole harmonic intensities and their phases as a function of the pulse propagation length. We have shown that, for low-order harmonics (up to $N \approx 11$), it is possible to coherently generate circularly polarized pulses shorter than the incoming incident circular pulse. Notice that the third harmonic, which in atmospheric linear laser filamentation [1,46] is an important nonlinear optical emission, is also observed in the LP-pulse propagations reported in Figs. 5–7. Of interest in our work, this now appears also in circular polarization. In fact, Fig. 10 shows that the third harmonic in circular polarization becomes more dominant with increasing gas density. In Fig. 13, this harmonic "splits" into a third and fourth harmonic, possibly due to Rabi oscillations. Macroscopic propagation effects on higher-order circular harmonics, and circularly polarized filaments, where strong inversion and laser emission has been observed from N_2^+ [47], are a future research direction. This will require extension of the present numerical MASP model through the inclusion of an additional nonhomogeneous transport equation for the macroscopic polarization coupled to Maxwell's equations [4,48].

ACKNOWLEDGMENTS

The authors thank Compute Canada for access to high-performance computer facilities for our simulations in highly nonlinear optics.

[1] S. L. Chin, *Femtosecond Laser Filamentation* (Springer, New York, 2010).
[2] E. Lorin, S. Chelkowski, E. Zaoui, and A. Bandrauk, Phys. D **241**, 1059 (2012).
[3] E. Lorin, S. Chelkowski, and A. Bandrauk, in *High-Dimensional Partial Differential Equations in Science and Engineering*, Vol. 41 of CRM Proc. Lecture Notes (AMS, Providence, Montréal, 2007), pp. 161–182.
[4] E. Lorin, M. Lytova, A. Memarian, and A. D. Bandrauk, J. Phys. A: Math. Theor. **48**, 105201 (2015).
[5] E. Lorin, S. Chelkowski, and A. Bandrauk, Comput. Phys. Commun. **177**, 908 (2007).
[6] P. B Corkum and F. Krausz, Nat. Phys. **3**, 381 (2007).
[7] P. B. Corkum, Phys. Rev. Lett. **71**, 1994 (1993).
[8] M. Lewenstein *et al.*, Phys. Rev. A **49**, 2117 (1994).
[9] A. D. Bandrauk, S. Chelkowski, and S. Goudreau, J. Mod. Opt. **52**, 411 (2005).
[10] A. D. Bandrauk, S. Barmaki, and G. L. Kamta, in *Progress in Ultrafast Intense Laser Science*, edited by K. Yamanouchi *et al.* (Kluiver, Amsterdam, 2006).

[11] M. Lein, J. Phys. B: At., Mol. Opt. Phys. **40**, R135 (2007).
[12] G. L. Kamta and A. D. Bandrauk, Phys. Rev. A **74**, 033415 (2006).
[13] E. Cunningham and Z. Chang, IEEE J. Sel. Top. Quantum Electron. **21**, 5 (2015).
[14] R. Velotta *et al.*, Phys. Rev. Lett. **87**, 183901 (2001).
[15] A. D. Bandrauk, H. Yu, S. Chelkowski, and E. Constant, Phys. Rev. A **56**, R2537(R) (1997).
[16] P. Lan, P. Lu, W. Cao, X. Wang, and G. Yang, Phys. Rev. A **74**, 063411 (2006).
[17] C. Vozzi *et al.*, Phys. Rev. Lett. **95**, 153902 (1995).
[18] J. Itatani *et al.*, Nature (London) **432**, 867 (2004).
[19] T. Kawai, S. Minemote, and A. Sakai, Nature (London) **435**, 470 (2005).
[20] A. D. Bandrauk, S. Barmaki, and G. L. Kamta, Phys. Rev. Lett. **98**, 013001 (2007).
[21] W. Cas, P. Lu, P. Lan, X. Wang, and G. Yang, Phys. Rev. A **74**, 063821 (2006).
[22] G. L. Yudin, S. Chelkowski, A. D. Bandrauk, and P. B. Corkum, J. Phys. B: At., Mol. Opt. Phys. **40**, F93 (2007).
[23] F. Theberge, N. Akozbek, W. Liu, A. Becker, and S. L. Chin, Phys. Rev. Lett. **97**, 023904 (2006).
[24] J. C. Painter *et al.*, Opt. Lett. **31**, 3471 (2006).
[25] M. B. Gaarde, M. Murakami, and R. Kienberger, Phys. Rev. A **74**, 053401 (2006).
[26] S. Chelkowski, C. Foisy, and A. D. Bandrauk, Phys. Rev. A **57**, 1176 (1997).
[27] A. D. Bandrauk and N. H. Shon, Phys. Rev. A **66**, 031401 (2002).
[28] H. S. Nguyen, A. Suda, and K. Midorikawa Phys. Rev. A **60**, 2587 (1999).
[29] A. D. Bandrauk, S. Chelkowski, and H. S. Nguyen, J. Mol. Struct. **735C**, 203 (2004).
[30] E. Lorin, S. Chelkowski, and A. Bandrauk, New J. Phys. **10**, 025033 (2008).
[31] T. Zuo and A. D. Bandrauk, Phys. Rev. A **54**, 3254 (1996).
[32] A. D. Bandrauk and H. Z. Lu, Phys. Rev. A **68**, 043408 (2003).
[33] S. Long, W. Becker, and J. K. McIver, Phys. Rev. A **52**, 2262 (1995).
[34] L. Mediauskas, J. Wragg, H. Van Der Hart, and M. Yu. Ivanov, Phys. Rev. Lett. **115**, 153001 (2015).
[35] J. M. Ngoko Djiokap, S. X. Hu, L. B. Madsen, N. L. Manakov, A. V. Meremianin, and A. F. Starace, Phys. Rev. Lett. **115**, 113004 (2015).
[36] A. Kamor, C. Chandre, T. Uzer, and F. Mauger, Phys. Rev. Lett. **112**, 133003 (2014).
[37] R. W. Boyd, *Nonlinear Optics*, 3rd ed. (Academic Press, Montréal, 2008).
[38] T. Brabec and F. Krausz, Phys. Rev. Lett. **78**, 3282 (1997).
[39] M. Geissler, G. Tempea, and T. Brabec, Phys. Rev. A **62**, 033817 (2000).
[40] Burnett *et al.*, Phys. Rev. A **45**, 3347 (1992).
[41] J. C. Strikwerda, *Society for Industrial and Applied Mathematics (SIAM)*, 2nd ed. (SIAM, Philadelphia, 2004).
[42] E. Lorin and A. D. Bandrauk, J. Comput. Sci. **3**, 159 (2012).
[43] K. J. Yuan and A. D. Bandrauk, J. Phys. B: At., Mol. Opt. Phys. **45**, 074001 (2012).
[44] E. Lorin, S. Chelkowski, and A. Bandrauk, Commun. Comput. Phys. **9**, 2 (2011).
[45] K. J. Schafer, B. Yang, L. F. Dimauro, and K. C. Kulander, Phys. Rev. Lett. **70**, 1599 (1993).
[46] F. Théberge, J. Filion, N. Aközbek, Y. Chen, A. Becker, and S. L. Chin, Appl. Phys. B: Lasers Opt. **87**, 207 (2007).
[47] P. Ding, S. Mitryukovskiy, A. Houard, E. Oliva, A. Couairon, A. Mysyrowicz, and Y. Liu, Opt. Express **22**, 29964 (2014).
[48] E. Lorin, M. Lytova, and A. Bandrauk, in *Laser Filamentation. Mathematical Methods and Models*, edited by A. D. Bandrauk, E. Lorin, and J. V. Moloney, CRM Series in Mathematical Physics (Springer, Montréal, 2016), pp. 167–183.